Laser texturing modelling using COMSOL Multiphysics ®

E.C. Chevallier[1], V. Bruyère[1], TianLong See[2], P. Namy[1]

[1] SIMTEC, 155 Cours Berriat, 38000 Grenoble, France
[2] Manufacturing Technology Centre (MTC), Ansty Park, Coventry, CV7 9JU, United Kingdom

1. Introduction

Surface engineering is a key technology used in a wide range of sectors in industry including biomaterials, power generation, offshore and electronics. The process involves adding functionality to a surface by texturing, i.e. altering the surface, or coating. The surface engineering market is currently dominated by surface coating, due to the higher level of maturity, high speed and relatively low costs associated with some of the techniques. However, in some industries, as medical implants manufacturing, where the durability is important, or when the use of harmful chemical is prohibited, for instance in food and drinks industry, surface coating may not be relevant and alternative techniques are required.

Laser surface texturing (LST) has emerged as a promising texturing technique due to properties such as excellent repeatability, non-contact process, the ability to achieve small-size features and high-quality finishing. Even though LST is a mature process, already available through a number of machine tool suppliers, its commercial applications are mainly limited to decorative rather than functional texturing. The work described here is part of the H2020 research programme called SHARK which aims at developing laser surface texturing from the current trial-and-error, lab-scale concept to a highly predictable, finite element (FE) modelling and data driven industrial approach. One of the challenges of the SHARK project is to overcome the lack of knowledge and resources available to inform the laser parameters selection. The aim of the work presented in this paper is to build an application using COMSOL Multiphysics® to predict the topography produced given the set of laser parameters as well as the material properties of the sample to be textured.

The aim of the model is twofold. First, it will allow the study of laser parameters influence such as power, frequency and pulse duration on the final topography. The second motivation behind the model development is the creation of an application using the Application Builder so that the surface topography prediction can be integrated in a laser machine, enabling the future user to predict the topography of one laser impact on its sample, using COMSOL Server™. The topography is further used in the machine to predict the surface functionality of the sample (wettability, friction coefficient etc.). In this paper, the modelling of a single laser impact is presented. A first ablation model built for this application is presented. The results are compared with experimental data to assess the validity of the approach and further development of the model, such as the fluid modelling are presented and discussed.

2. Laser ablation numerical modelling

Model geometry

The FE model presented in this work was developed with COMSOL Multiphysics® version 53a. As the topography of a single crater after one impact is simulated, the model geometry is 2D-axisymmetric. The geometry of the model is presented in Figure 1. The dimensions are set to depend on the laser spot size referred to as r_{spot} in Figure 1.
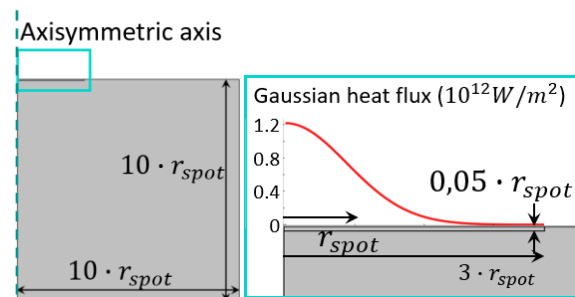

Figure 1: 2D axisymmetric model, dimensions and detail. The Gaussian heat flux magnitude is represented on the solid gas interface.

Thermal problem

The laser-material interaction is time-dependent, as heating and subsequent cooling need to be modelled. The temperature evolution is predicted by solving the time dependent energy equation, through its conduction form:

$$\rho C_p \frac{\partial T}{\partial t} + \nabla \cdot (-k\nabla T) = 0$$

where T is the temperature, k is the thermal conductivity, ρ, the density and C_p the specific heat at constant pressure.

The energy deposition is assumed to be Gaussian and is modelled by a boundary heat flux, as presented in Figure 1. The thermal inward heat flux is formulated as:

$$-\boldsymbol{n} \cdot (-k\nabla T) = P_{laser} \cdot \frac{A_0}{\pi\left(\frac{w_0}{2}\right)^2} \cdot e^{-\frac{r^2}{\left(\frac{w_0}{2}\right)^2}}$$

where P_{laser} is the peak laser power, A_0, the surface absorptivity, r, the radius and w_0, the beam waist.

The peak laser power is computed from the average power P_{ave} and the power time distribution obtained from experimental data from [1]. As the average power is the average of the laser power over a period, P_{laser} should satisfy the following equation:

$$P_{ave} \cdot \frac{1}{f} = \int_{t\in[0;\frac{1}{f}]} P_{laser} \cdot f_{deposition}(t)dt$$

where f the frequency of the laser pulses and $f_{deposition}$ is the power time distribution (unit-less quantity), represented in Figure 2, where the pulse duration is referred to as τ_{laser}. On the other boundaries of the model, thermal insulation is assumed, by forcing the normal conductive flux to be null:

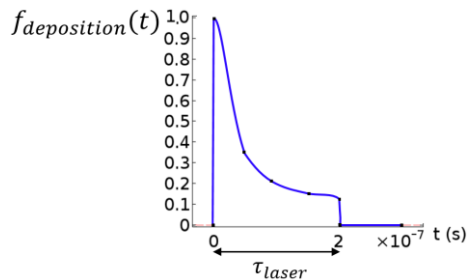$$-\boldsymbol{n} \cdot (-k\nabla T) = 0$$

Figure 2: Time dependent power distribution function. Data are extrapolated from [1].

Ablation modelling

In this model, only the solid phase is modelled meaning the gas around the component and the vaporised matter are not simulated. This choice of modelling also implies the mass is not conserved. In order to compute the shape of the solid component after one laser impact, the assumption that the solid material surface temperature not exceeding the vaporisation temperature T_{vap} significantly is made. In the model, this assumption is expressed by the use of the convective flux boundary condition defined as:

$$\Phi_{vap} = h(T - T_{vap})$$

where Φ_{vap} is the vaporised flux, h is a numerical parameter and T_{vap} is the vaporization temperature.

At the solid gas interface, the energy balance is assumed and is expressed as:

$$\rho L_v \boldsymbol{u_{vap}} \cdot \boldsymbol{n} = \Phi_{vap} \cdot \boldsymbol{n}$$

where L_v is the latent heat of vaporization, $\boldsymbol{u_{vap}}$, the velocity of the matter leaving the interface and $\boldsymbol{n}$ the normal vector of the solid front.

The surface is considered free to move to accommodate the change in geometry due to the matter loss. The Deformed Geometry interface is used by setting the normal mesh velocity v_n at the solid gas interface to:

$$v_n = \Phi_{vap}/(\rho * L_v)$$

Mesh

A mapped (regular) mesh of quadratic elements is used in the refined region in the top left rectangle, as presented in Figure 1, whereas a triangular coarser mesh is used elsewhere. The size of the elements in the small region is set as large as possible to avoid excessive element distortion yet fine enough to capture the temperature gradient. At each time-step, the displacement of the moving boundary is propagated throughout the domain using Laplace mesh smoothing technique which minimises the displacement difference between two neighbour nodes.

Material properties

The simulation and experiments presented in this paper were performed on AISI 316L austenitic stainless steel, a well-known material widely used in industry. A density of $\rho = 7966 \, kg/m^3$ is used in the model, along with an absorptivity value of $A_0 = 0.5$ and a latent heat of vaporization of $L_v = 6 \cdot 10^6 J/kg$. Temperature dependent properties from ambient to melting point from [2] are used in the model for k and

C_p values. The values are reported in Table 1 and linear approximation are used to interpolate the values.

Table 1: Thermal material properties used in the model, values from [2].

Temperature (°C)	Specific Heat (J/kg/K)	Thermal conductivity (W/m/K)
20	492	14.12
100	502	15.26
200	514	16.69
300	526	18.11
400	538	19.54
500	550	20.96
600	562	22.38
700	575	23.81
800	587	25.23
900	599	26.66
1000	611	28.08
1100	623	29.50
1200	635	30.93
1300	647	32.35
1400	659	33.78

Time dependent solver

The scales involved in the process vary from nanoseconds (during the laser pulse) to tens of microseconds (duration of one period) which causes the problem to be multi-scale in time. This requires a careful setup of the time step during the resolution, especially when the gradient of the heat flux deposited with time is large, i.e. at the beginning of the impact. During the impact, the time step should be fine enough to capture this (very short) deposition. Then, when the material cools down, the time step should be increased to avoid excessively long computational times, as the ratio of the cooling time over pulse duration is typically 1:10.

3. Experimental work

Dedicated experimental work was performed to validate the results from the model presented in section 2. The tests were performed by the Manufacturing Technology Center, MTC in Coventry, which is one of the partners and project coordinator of SHARK. The experimental parameters were selected to provide sufficient data to compare with the FE predictions and subsequently inform on the validity of the hypothesis and modelling approach selected.

The laser machine used to perform the experimental tests is a GF laser P 400 machine using an Ytterbium fibre laser source with a wavelength of 1064 nm. In the set of tests presented in this paper, the frequency and duration of pulses are set respectively to 30 kHz and 200 ns for all the tests while the average output powers varies from 2.73 W to 27.18 W. The speed is set so individuals impacts are produced, here $3\ m/s$. 3D contour images and line scan data profiles of the craters were produced using a confocal microscope. A crater image and line scan from sample no. 4 are presented in Figure 3.

Table 2: Experimental samples and laser parameters

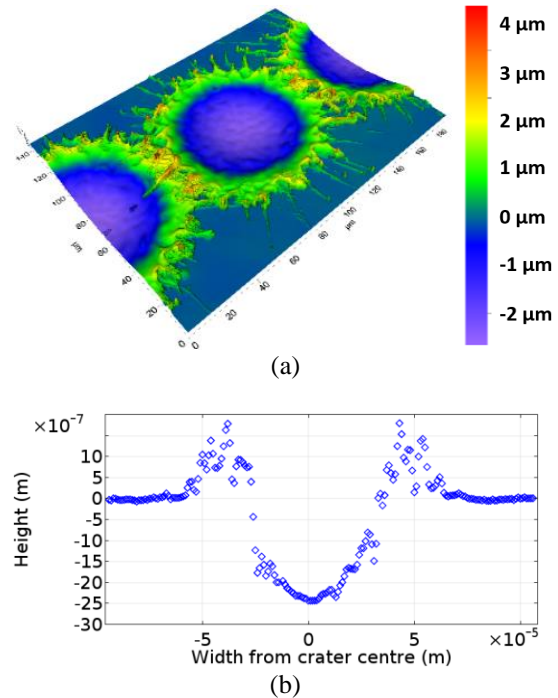| Sample no.	Average power (W)	Speed (m/s)	Frequency (kHz)	Pulse duration (ns)
1	2.73	3	30	200
2	9.06	3	30	200
3	13.59	3	30	200
4	19.02	3	30	200
5	27.18	3	30	200

(a)

(b)

Figure 3: 3D contour (a) and profile scan line (b) from sample no.4

4. Ablation model results and discussion

The validity of the modelling approach was assessed by comparing the predicted topography with the experimental measured topography for the five cases presented in section 3. The topography elements of

comparison are the crater radius and depth. As it can be seen in Figure **3**, the experimental craters are surrounded by a peak hence the crater diameter is measured by considering the peak-to-peak distance. On the other hand, as the FE model does not predict a peak as only the ablated matter is considered, the crater radius is defined as the distance from the centre to the fusion line, on the top surface of the model.

In Figure 4, the measurements of the crater radiuses are plotted along the FE melt pool radiuses predictions against average power values and it can be seen the results are in good agreement both in terms of magnitude and evolution tendency, with less than 12% difference for samples 2 to 5. The FE predicted radius for sample 1 is considerably overestimated however the radius gradient in this power range is steep and it can be seen the experimental value does match the FE prediction curve tendency. The good agreement between predicted and experimentally measured radiuses indicates satisfactory thermal predictions.

In Figure 5, the depth of the craters of each experimental case is plotted along the depth predicted by the FE model in a given range of average power values. Both predicted and experimentally measured depth values are of the order of magnitude of microns, however, it can be seen that the trend predicted by the FE model is linear whereas the experimental results is non-linear. This comparison informs the need of taking into account physics which are not considered in the model, such as fluid dynamics.

The predicted and measured sample crater profiles for no. 4 are plotted on the same graph in Figure 6 for comparison. It can be noticed that the diameter and depth of the predicted and experimental craters correspond. However, the experimental craters are surrounded by a peak which is not predicted by the FE model. The peak is likely due to re-deposition of vaporised matter after the impact, or from the migration of molten material to the edge of the crater.

In the next section, a thermo-hydraulic model of the laser impact, with no ablation modelling is presented and preliminary results indicate peaks of the same order of magnitude than that observed experimentally are predicted. This information is of particular importance to the application, as peaks of the same order of magnitude as the crater depth- will influence the surface functionality hence must be predicted by the model.
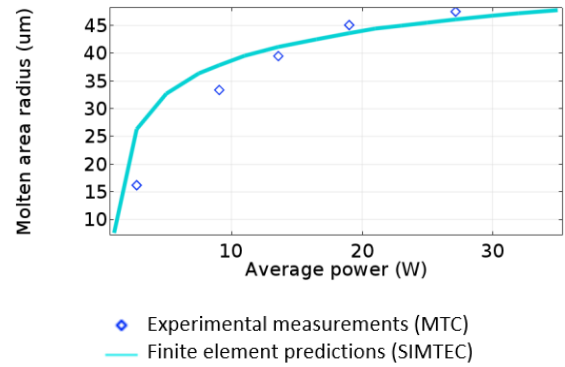

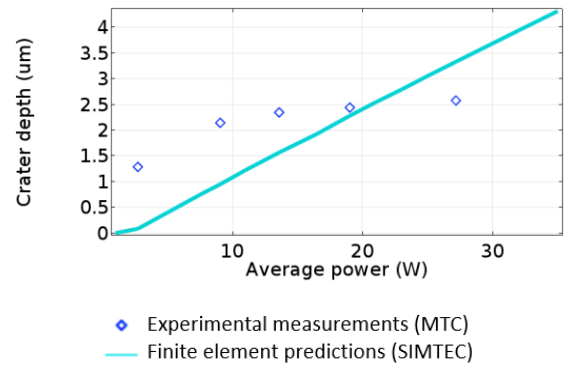**Figure 4:** Molten area radius evolution with average power.

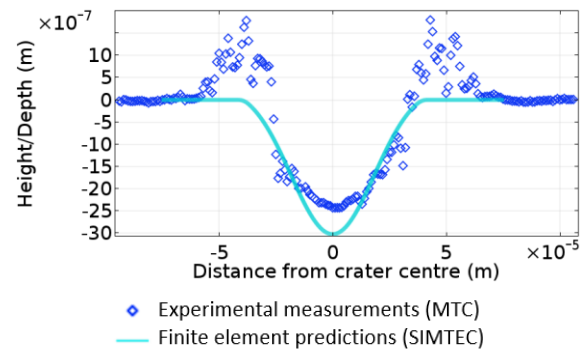**Figure 5:** Crater depth evolution with average power.

Figure 6: Experimental measurements from MTC (diamonds) and laser ablation FE prediction (full line) of the crater profile from sample no. 4.

5. Thermo-hydraulic fluid numerical modelling

In this section, a different laser-material interaction modelling approach is proposed. It involves the simultaneous fluid temperature, velocity and pressure computation during the time-dependent process. A range of physical phenomena in the fluid domain will influence the final shape of the resulting crater. Before temperature reaches vaporisation temperature,

the laser beam interacts with an almost flat surface [3]. When the vaporisation temperature is reached, the ejected vapour induces a pressure called the recoil pressure [3] which pushes the fluid downwards and subsequently creates the crater shape.

Thermal problem

The time dependent temperature evolution is predicted in the domain by solving the Energy equation in its convection/diffusion form:

$$\rho C_p \left(\frac{\partial T}{\partial t} + (\boldsymbol{u} \cdot \nabla)T \right) = \nabla \cdot (k \nabla T)$$

where $\boldsymbol{u}$ denotes the velocity field.

The thermal boundary conditions, including the laser energy distribution are as described in section 2.

Fluid modelling

The transport of mass and momentum, governed by the Navier-Stokes equations, is solved in the fluid domain for a laminar and transient incompressible fluid flow:

$$\begin{cases} \nabla \cdot \rho \boldsymbol{u} = \boldsymbol{0} \\ \rho \left(\frac{\partial \boldsymbol{u}}{\partial t} + (\boldsymbol{u} \cdot \nabla)\boldsymbol{u} \right) = \\ \quad \cdot \left[-p\bar{\bar{I}} + \eta(\nabla \boldsymbol{u} + \nabla \boldsymbol{u}^T) - \frac{2}{3}\eta(\nabla \cdot \boldsymbol{u})\bar{\bar{I}} \right] + \rho \boldsymbol{g} \end{cases}$$

with p the pressure and η the fluid dynamic viscosity.

At the liquid gas interface, the recoil pressure p_{recoil} is applied when the temperature exceeds T_{vap}. In literature, several models were developed to quantify the recoil pressure using adaptations of the Clausius-Clapeyron law [4-5]. In this work, the approach selected is a simplified law

$$p_{recoil} = Ae^{-\frac{r^2}{\left(\frac{w_0}{2}\right)^2}}$$

where A is a numerical parameter.

In the fluid, normal surface tension forces (Laplace forces) counter the recoil pressure action while near the irradiated surface, Marangoni effects influence the enlargement of the welding pool.

The liquid gas interface evolution is controlled by the recoil pressure, surface tension and Marangoni effects which vary during the laser pulse. An ALE (Arbitrary Lagrangian Eulerian) method is used along with a Laplace mesh smoothing method is used to allow the fluid surface to deform.

In this simulation, the solid is assumed to behave as a fluid of higher viscosity μ_{sol} than that of the fluid, μ_{liq} when the temperature is below the melting temperature of the material, T_{melt}. In the model, $\mu_{sol} = 1 \text{ Pa} \cdot \text{s}$ and $\mu_{liq} = 10^{-3} \text{ Pa} \cdot \text{s}$.

6. Thermo-hydraulic fluid modelling preliminary results and discussion

As a preliminary result, the crater profile obtained for sample no. 4 is presented in Figure 7 along with the experimental measurements. It can be seen that a peak is predicted and for that particular case, the results show a satisfactory agreement. This preliminary result is encouraging as it informs on the preferred approach to use to predict the crater peaks observed experimentally. It is emphasised here that these results match the experimental data for that case in particular and are presented here to demonstrate the approach selected, however it is not the case for all set of parameters tested and further work is required to reach such a comparison for the other samples.

In the thermo-hydraulic model, the vaporisation of the matter was not included, which means the volume is conserved. However, according to the energy provided to the sample, some matter may be ablated. Hence, to achieve a model that predicts laser ablation, experimental data on the amount of matter vaporised is required. This data is extremely difficult to obtain as it requires experimental measurements of volumes of the order of magnitude of $10^{-16}m^3$. Alternative approaches to model laser ablation will be investigated in the future.
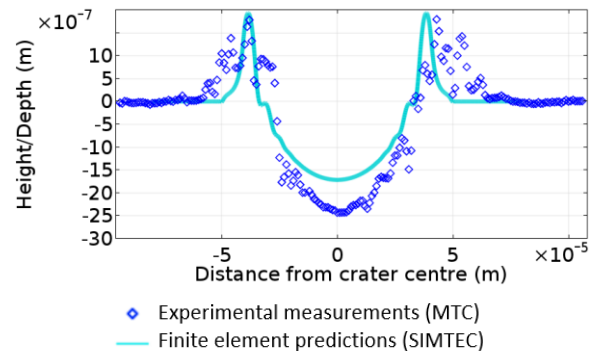

Figure 7: Experimental measurements from MTC (diamonds) and thermo-hydraulic FE model prediction (full line) of the crater profile from sample no. 4.

7. Topography prediction application

One of the motivations behind the laser-material interaction model development is to create a topography prediction tool integrated in the laser machine that will predict the topography of one impact

on a flat surface from a set of laser parameters, material properties and operating conditions. As the user is not necessarily familiar with the FE technique and modelling in general, the tool should be set up for cases where the hypothesis of the model are valid.

An application from the ablation model presented in section 2 was created using the Application Builder of COMSOL Multiphysics®. The output of the application are the crater profile, width and depth. As it was reported, the crater is surrounded by a peak which is likely to influence the surface functionality. It was observed that further development of the model allow the peak prediction by involving the fluid flow.

8. Conclusions

In this paper, a technique to model laser ablation was presented. The technique is based on the assumption that the surface temperature do not exceed vaporisation temperature significantly. The energy balance equation at the solid gas interface is used to derive the vaporised matter flux velocity, which is input as the normal mesh velocity. The temperature in the model was computed by solving the time dependent Energy equation and the laser heating was modelled by a time-dependent Gaussian heat source. The results from the thermal model are in good agreement with the experimental results. However, the modelling of the ablated matter is not sufficient to predict the topography of the textured surface accurately after one laser impact as molten material behaviour plays a significant role in the crater shape. The effect of the fluid on the crater topography is considered in the second model, which involves solving a coupled thermo-hydraulic problem, allowing peak prediction, which is essential to accurately predict the surface functionality.

As for the use of the ablation modelling, it was clearly demonstrated in this paper that this method cannot be used on its own to predict crater topography due to the presence of fluid. The modelling of matter ablation will be use together with the fluid modelling to predict the crater topography and the method will be compared against experimental measurements for validation. Future work will involve assessing the validity of the model for other materials and operating conditions, such as the pulse duration, frequency and average power. The influence of the initial surface on the predicted topography will also be assessed and taken into consideration in the model.

10. References

1. D. Gilbert, M. Stoesslein, D. Axinte, P. Butler-Smith and J. Kell, A time based method for predicting the workpiece surface micro-topography under pulsed laser ablation, *Journal of Materials Processing Technology*, **214**, 3077-3088 (2014)
2. S. K. Bate, R. Charles and A. Warren, Finite element analysis of a single bead-on-plate specimen using SYSWELD, *International Journal of Pressure Vessels and Piping*, **86**, 73-78 (2009)
3. V. Bruyère, C. Touvrey and P. Namy, Comparison between phase field and ALE methods to model the keyhole digging during spot laser welding. Proceedings from the 2013 COMSOL Conference in Rotterdam
4. W. Semak, W.D. Bragg, B. Damkroger and S. Kempkas, Temporal evolution of the temperature field in the beam interaction zone during laser-material processing, *Journal of Physics D: Applied Physics*, **32**, 1819-1825 (1999)
5. C.J. Knight, Theroretical modelling of rapid surface vaporization with back pressure, *American Institute of Aeronautics and Astronautics*, **17:5**, 19-523 (1979).